Int J Adv Manuf Technol (2017) 91:1839–1849
DOI 10.1007/s00170-016-9851-2

ORIGINAL ARTICLE

Mechanical properties of a novel plymetal manufactured by laser-assisted direct metal deposition

Sohaib Z Khan[1,2] · **S.H. Masood**[1] · **Ryan Cottam**[1]

Received: 14 July 2016 / Accepted: 29 November 2016 / Published online: 24 December 2016

Abstract Plymetal is the term used here to describe a composite structure where more than one solid metals are joined or pressed to gain unique set of properties. Mostly flat plates are used, which are then bonded together to form sheets for further forming processes. In this work, a novel plymetal is designed to create a structure with alternating layers of metals both in radial and in axial directions. In the radial direction, the plymetal was conceived by having a cylinder surrounded by annular structure of alternate material. In the axial direction, the centre cylindrical material is changed, followed by annular structure of alternate material. Such a plymetal is realised by laser-assisted direct metal deposition additive manufacturing technology. Two different metal powders, AISI H13 tool steel and AISI 316L stainless steel, were used to create the plymetal. The uniaxial compressive test was performed on the plymetal, and the results were compared with the individual solid structure of H13 tool steel and 316L stainless steel, also made by direct metal deposition. Young's modulus, yield strength and yield strain of the samples were determined in compression. The dual modulus of elasticity in the region before yielding was observed in all samples. An analytical equation to calculate Young's modulus of the plymetal based on a stiffness method was also derived. Microstructure of the plymetal was observed through optical and scanning electron microscopy, which revealed perfect bonding between the two metals and small pores with sizes less than 1 μm. It is expected that the variant of plymetal will be able to give better tuneable control on the mechanical properties for numerous applications.

Keywords Direct metal deposition · Lasers · Plymetal · 316L · H13 · Composite

✉ S.H. Masood
smasood@swin.edu.au

[1] Faculty of Science Engineering and Technology, Swinburne University of Technology, Hawthorn, VIC 3122, Australia

[2] Department of Mechanical Engineering, Faculty of Engineering, Islamic University of Madinah, MadinahPO Box 170, Kingdom of Saudi Arabia

1 Introduction

In many engineering applications, existing monolithic alloys and metals put restrictions on material selection for specific design due to their limited properties and characteristics. In a desire to control physical and mechanical properties of materials, researchers are pushing the boundaries to form new materials, composites, alloys and different structures. This provides greater flexibility for the selection of materials for particular engineering design applications. Inducing microstructural and macrostructural changes in the material is one of the methods to improve properties of materials [1]. Even monolithic alloys and metals can be given different structures, for example, cellular, porous or foam-like structures, which provide tenable control to achieve desired set of properties [1–3].

There are many models of composite material that provide better control on properties by mixing two or more constituents, for example, metal matrix composites (MMCs). In case of MMC, the base material is metal, which is reinforced with particles, platelets, continuous and non-continuous fibres [4–6]. In MMC, the particulate inclusions for reinforcement are generally made up of metal-based carbides, nitrides, borides and oxides, whereas the fibre inclusions are generally made up of alumina and carbon [4]. A hybrid approach has also been used by mixing particulates and fibres together in a single MMC [7]. The use of long alumina fibre in Al-6061 MMC is

reported to improve fracture stress by more than 50%, which depended on fibre orientation and strain rates [5]. Reinforcement in MMC generally improves isotropic properties of the materials; however, in case of fibres in MMC, the properties are still affected by the direction of the fibres [5, 8]. Another class of composite materials is the sandwich structures in which a different low-density cellular or porous core is sandwiched between thin plates [9]. Sandwich structures are the most suitable when the weight of the load-bearing component is critical. By changing the size and dimension of the core and the plate, desire results can be achieved. Other more advanced materials can be classified as multifunctional material system [10]. Examples of the multifunctional materials are functionally graded materials (FGMs), which are generally manufactured by conventional processes of powder metallurgy or melt processing [11]. In FGM, composition and structure of the constituent materials are gradually varied over the bulk volume. This results in a gradual change of the structure of material and thus gradual change in corresponding properties along the variational direction of the material. Metal and ceramic (ductile and brittle) layered structures have also been studied to improve the fracture resistance of the composite [12]. These metal/ceramic composites have many applications, especially in electronic industry.

The manufacturing of appropriate composite structure is the basic hindrance in realising metal-based composites. The most commonly used processes for the manufacturing of metal-based composite materials (or MMCs) are derived from casting techniques and powder metallurgy methods [4, 13]. Multi-layered composite materials can be manufactured by severe plastic deformation (SPD) techniques [14, 15]. In SPD techniques, layers of different materials are pressed together, which not only deform these layers but also create bonds between them. Deformation or rolling process can be repeated many times to form the final structure of the material. Bulk materials with sub-micron grain size are possible to obtain through specialised SPD techniques [14]. Homogenous material composition can also be achieved by SPD techniques. In Al/Ni composites, fragmented nickel layers were found to be homogenously mixed in aluminium matrix by the accumulative roll bonding [15]. Multi-layered composite structures can also be manufactured by diffusion bonding under high temperature and compressive load [12]. The properties of the layered structure metals at the diffusion boundaries can be controlled with the addition of another material different from the materials used to form layered structure [16, 17]. For example, during diffusion bonding, Ag was added between the layers of Ti6Al4V and AISI 304 stainless steel, which resulted in obtaining defect-free bonds [16]. Similarly, thin Cu layer was added between the layers of titanium and stainless steel, which resulted in reduction of diffusion time and also blocked a chemical reaction between the base materials [17].

In contrast to the conventional material removal or deformation processes, additive manufacturing (AM) techniques provide an alternate way in which a part is manufactured via layer-by-layer addition of material [6, 18]. Multiple AM techniques have allowed a bottom-up approach of manufacturing components in different fields of applications [19]. The major advantages of AM techniques over conventional methods include possibility of manufacturing significantly complex components and

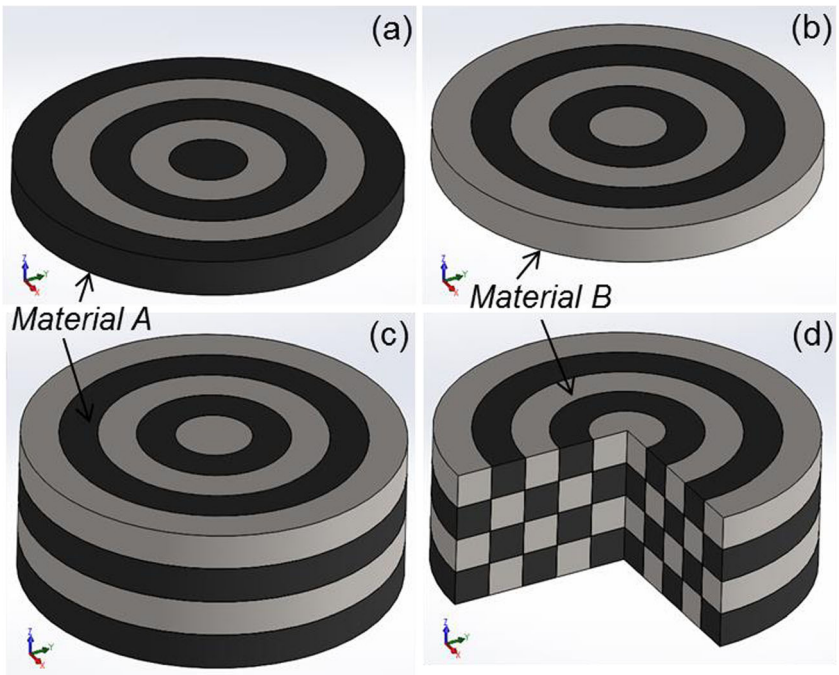

Fig. 1 Conceptual plymetal model showing **a** first layer zone, **b** second layer zone, **c** assembly of four layer zones and **d** inside view of the plymetal

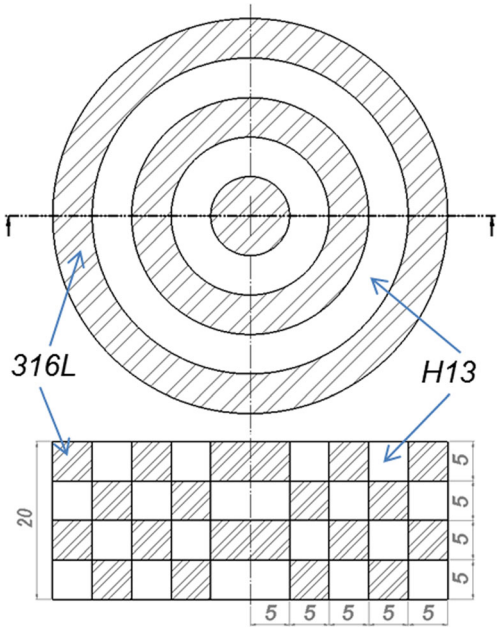

Fig. 2 Drawing of the sample plymetal with cross-sectional view. All dimensions in millimetres

having tailored composition [20]. In additive manufacturing, multi-material components can be manufactured by several techniques, such as by depositing different materials by a laser powder deposition (LPD) technique through feeders [21] or by allowing wire feed with the powder during deposition [22]. In LPD-type AM techniques, the input material for a part manufacturing can be altered within each layer during the metal deposition to make unique materials [21]. This inherent feature of LPD-type AM has made it possible to make solid structures with variant materials, such as MMC and FGM. In manufacturing multi-material component, the basic idea is to create a bond between different metals to form a new structure. Generally, high cooling rates in the range between 10^3 and 10^{11} K/s are possible during laser processing AM technologies [23]. The control on metal deposition during AM also allows to form interlink of multiple metals rather than particulate or fibre inclusions to manufacture metal-based composites.

Direct metal deposition (DMD) is a LPD AM process, in which a focused laser beam is used to fuse metal powder by melting and depositing it on a base substrate or on the previous layer [24]. The CO_2 laser is most commonly used in DMD, as it provides more power and control on the overall process. The DMD process is suitable for fully dense part fabrication as well as for repair of tools and components. Some studies have also focused on deposition of one metal on another metal by DMD to achieve desired properties and performance. Imran et al. [25] investigated deposition of H13 tool steel on high-strength Cu alloy substrate using DMD both with and without using 41C stainless steel as a buffer layer material for bimetallic tooling application. In another report, Erinosho et al. [26] investigated optimal DMD process parameters for the improved bonding between Cu and Ti6Al4V alloy composite. The DMD process and other similar LPD AM processes like laser engineered net shape (LENS) and direct laser fabrication (DLF) have also been used to generate FGM and compositionally graded structures using two different metals. Soodi et al. [21, 24] developed both functionally graded structure and wafer layered structure by the laser-assisted DMD technology and investigated the changes in tensile strength and coefficient of thermal expansion (CTE) using pairs of metal from a range of engineering alloys (316 SS, 420 SS, Stellite 6, Aluminium Bronze, Colmonoy 6, H13 tool steel), which are used in different engineering applications. Pulugurtha [27] fabricated functionally graded thin wall structures involving Ti6Al4V and Inconel 625 alloys by a laser DMD for space heat exchanger application taking advantage of high-strength/weight ratio of Ti6Al4V and high temperature oxidation resistance of Inconel 625. Shah et al. [28] have used laser DMD system to develop FGMs involving Inconel 718 and 316L stainless

Table 1 Laser-assisted direct metal disposition process parameters

Description	Units	Plymetal	H13	316L
Laser power	W	2200	3000	3000
Laser beam diameter	mm	1	2.5	2.5
Laser power density	W/mm^2	2800	610	610
Scan speed	mm/min	325	250	250
Powder diameter	μm	50–150	50–150	50–150
Powder feed rate	g/min	8.1 for H13 7.5 for 316L	12.5	12.5
Shielding gas (Argon)	L/min	10	10	10
Layer thickness	mm	0.65–1.30	1.7	2
Overlapping	–	Half-track	Half-track	Half-track
Laser mode	–	Continuous	Continuous	Continuous

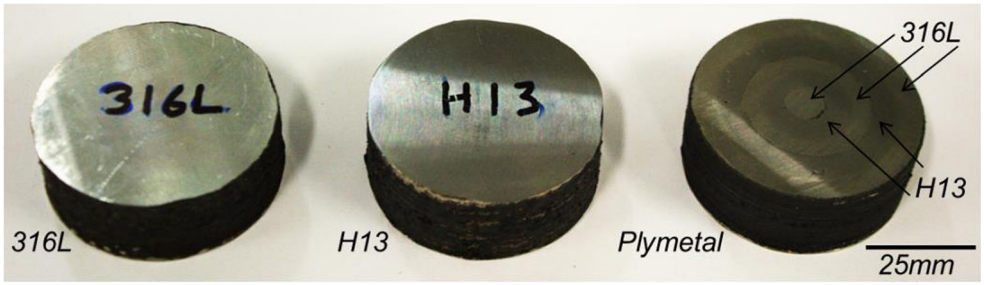

Fig. 3 Samples after manufacturing by laser-assisted direct metal deposition. Alternating metals are visible in plymetal sample

steel and investigated the effect of process parameters on hardness, wear resistance and tensile strength. Balla et al. [29] applied a LENS process to fabricate FGM structures using pure Ti and TiO_2 and noted that these structures significantly increased the surface wettability and hardness. Liu and DuPont [30] also used the LENS system to fabricate ceramic/metal FGM involving TiC and Ti and analysed hardness distribution. Articek et al. [31] have applied LENS technology to develop FGM for tooling application using H13 tool steel and copper exploiting high wear resistance of tool steel and high thermal conductivity of copper for better thermal management. Wang et al. [32] used a DLF process involving powder and wire feed to fabricate compositionally graded materials using Ti6Al4V wire and TiC powder aimed at improving wear resistance. Hofmann et al. [33] have used a laser deposition system (LDS), similar to LENS, to develop gradient metal alloys through a radial deposition technique using Ti6Al4V alloy and vanadium powders with focus on low CTE. Chu and Yu [34] proposed a methodology to determine the material composition in FGM using a multi-criteria decision making method based on computer-aided engineering analysis. Hofmann et al. [35] have provided an overview of the development of compositionally graded metals using metal AM and have proposed a systematic roadmap for alloy design based on AM techniques and required physical properties with desired functionality.

Published works have shown that LPD processes like DMD have been tried extensively to fabricate functionally graded structures for different applications. However, very little attention has been paid on development of novel multi-material composite structures for which DMD-type AM process is equally suitable.

In this study, a novel plymetal composite structure is designed and realised by laser-assisted DMD technique. Two different metals were used to make a cylindrical-shaped plymetal sample. Mechanical properties under uniaxial compression were investigated on plymetal and compared with the properties of the individual metal samples of the same size. Young's modulus, yield strength and yield strain of the samples were determined, and an analytical model for stiffness of plymetal is proposed. Hardness of both metals in the samples was also measured and compared with the literature. A microstructure analysis of the plymetal was carried out using optical and scanning electron microscopes.

2 Methods and material

2.1 Conceptual plymetal model

Plymetal is the term used when there are more than one solid metals joined or pressed together to gain unique set of properties. Mostly flat plates are used, which are then bonded together to form sheets for further forming processes. The properties of such structures are mostly limited to the normal direction of the layers. In this study, the concept was to create a plymetal with alternating layers of metals both in radial and in axial directions. In the radial direction, the plymetal was conceived by having a cylinder surrounded by annular structure of alternate material as shown in Fig. 1a. In the axial direction, the centre cylindrical material is changed, followed by annular structure of alternate material as shown in Fig. 1b. The whole structure is defined by two-layer zones, which can be considered as a unit cell that can be repeated in axial direction to create the whole structure. Multiple configurations are possible in terms of dimensions, the number of materials and in the fashion that they are being altered. However, in this

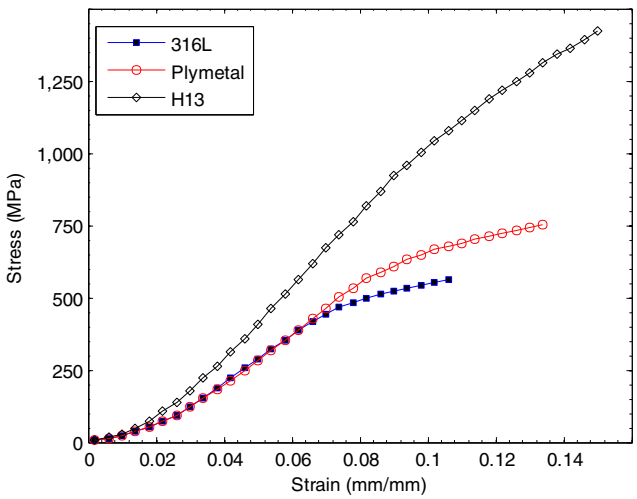

Fig. 4 Stress and strain curve of the compression test

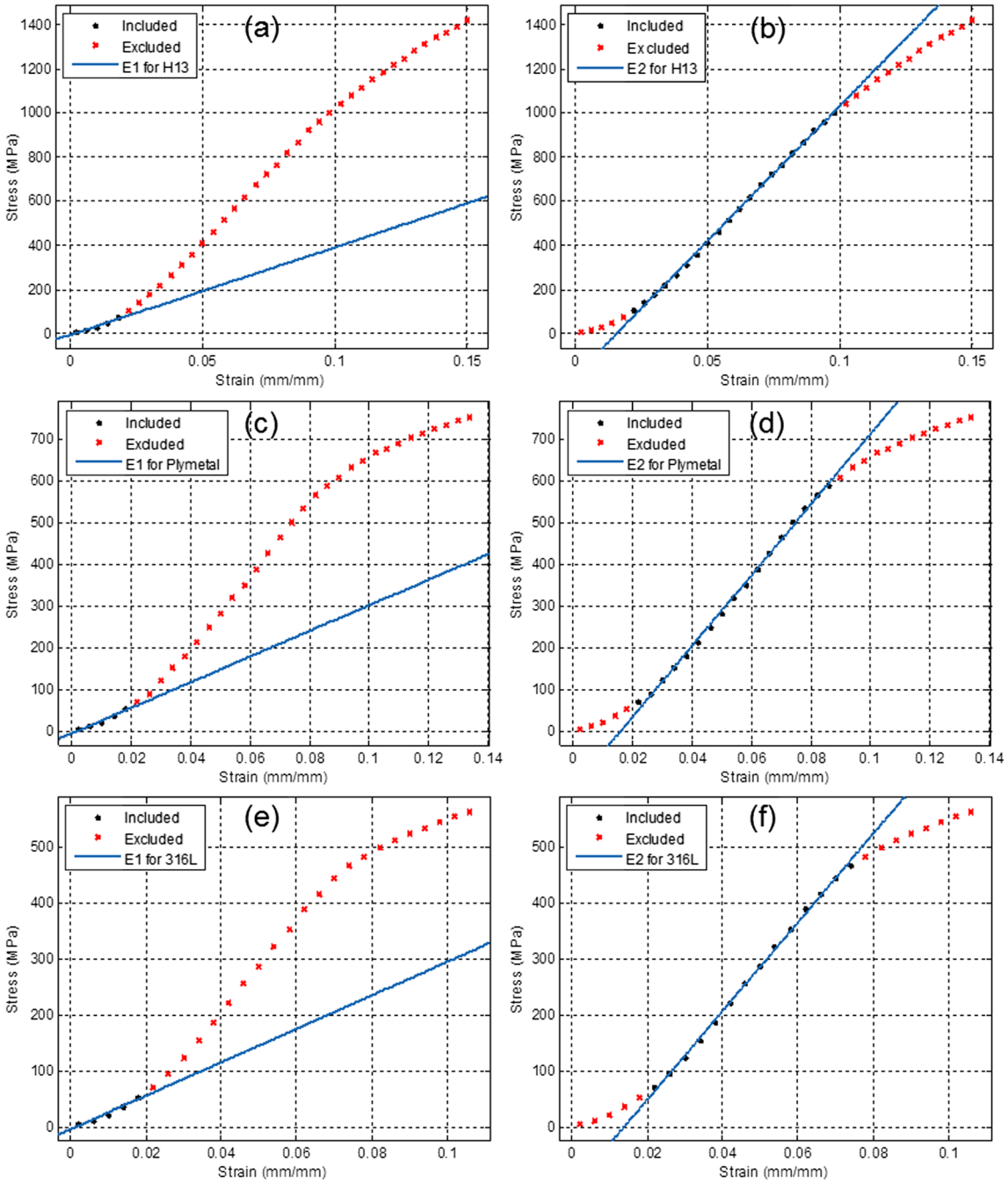

Fig. 5 Estimation of E1 and E2 from the compression test on the segmented data sets

work, the concept is restricted to two materials with total four layer zones as shown in Fig. 1c. Each zone should have the same dimensions, and both materials are enclosed by each other as shown in Fig. 1d.

Table 2 Uniaxial compression test results

Sample material	R^2 for linear curve fitting		Young's modulus		Yield strength (MPa)	Yield strain
	for E1	for E2	E1 (GPa)	E2 (GPa)		
H13	0.9987	0.9647	3.97	12.23	1100	0.105
Plymetal	0.9980	0.9698	3.06	8.45	600	0.087
316L	0.9986	0.9685	2.99	7.92	478	0.074

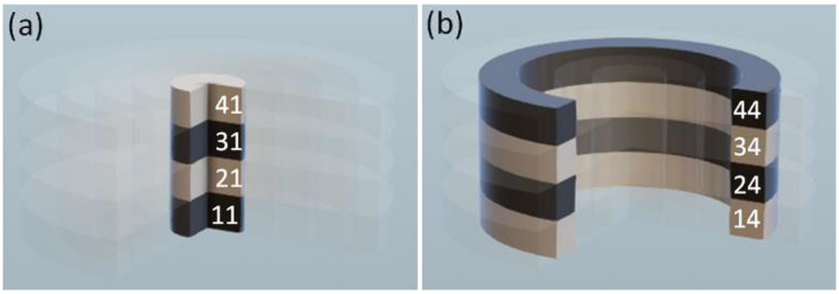

Fig. 6 Cut section showing series configuration of the plymetal for **a** middle portion and **b** annular portion

2.2 Manufacturing of the plymetal

The dimensions of the plymetal sample as derived from the concept design are shown in Fig. 2. For property comparison purpose, separate solid cylinders of each metal were also manufactured with dimensions of 25-mm radius and 20-mm height.

The machine used for the manufacturing of the structure by DMD was POM DMD 505, operating with a CO_2 laser with a maximum laser power of 5 kW. The two metals used in this study were AISI H13 tool steel and AISI 316L low-carbon stainless steel. Both metals were in powder form used to make solid structure. The chemical composition of the metal powders can be seen in [36]. Three different samples were manufactured: plymetal, H13 and 316L The materials for plymetal include alternate ring layers of H13 and 316L steel as discussed in the previous section. The material details and parameters used for manufacturing the samples are summarised in Table 1.

After each layer deposition, the thickness of the layer was measured. For plymetal, the initial layers were having smaller thickness, but as the part was built in vertical direction, the layer thickness was increased. A half-track overlapping was set for all the scans during the deposition. Track overlapping minimises porosity and voids in the samples during laser deposition [37]. Once the samples were manufactured, they were machined from the base plate and also machined from the top to maintain the design dimensions. The final samples after machining are shown in Fig. 3. It should be noted that the alternate layers of H13 and 316L for the top surface are visible as the darker rings for H13 and the lighter rings for 316L in the plymetal sample. The density of each sample was approximately 7.5 g/cm^3 measured by weighing the sample and divided by the volume of the samples.

2.3 Uniaxial compression test

A uniaxial compression test was performed using an Instron four-column static testing machine with the maximum load capacity of 5 MN. The samples were placed between the hardened flat platens of the machine and compressed along the thickness (build direction) of the sample. The test was performed on each sample beyond yielding at a constant strain rate of 1 mm/min. The compressive strain was obtained directly from the machine using an extensometer attached with the platens. The compressive stress was obtained by dividing the applied force by the cross-sectional area of the sample.

2.4 Sample preparation for microanalysis

The top surface of the samples was ground and polished for microanalysis. The mechanical grinding of the samples was performed on a silicon paper under flowing water. The grit sizes of the papers used for grinding were 120, 180, 240, 320, 600 and 1200. The polishing was carried out by using a diamond-based suspension on polishing cloth with particle sizes of 6, 3 and 1 μm.

For microstructure analysis, the plymetal polished surface was chemically etched with H_2O/HCl/HNO_3 (1:1:0.2) solution for approximately 3 s. The surface was then rinsed and dried with ethanol. Microstructures were observed with optical microscope (Olympus BX61) at various magnifications. A scanning electron microscope (SEM) (Zesis Supra 40VP) was used for the observation of microstructure at higher magnifications.

3 Results and discussion

3.1 Uniaxial compression test

There are two types of Young's modulus reported in literature for the tension test of alloys, mostly for porous structures [38]. The first one is termed as the 'true Young's modulus' (E1), as this can be measured by other techniques, for example, ultrasonic test [39]. The other one is termed as 'apparent Young's

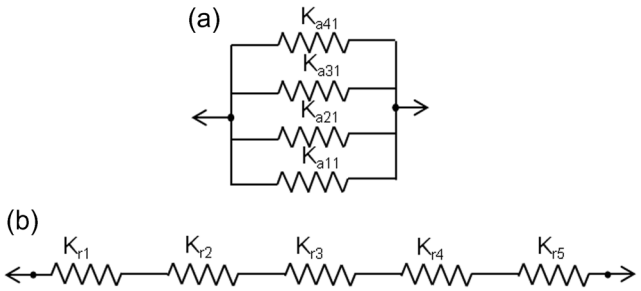

Fig. 7 Analogues circuit for **a** series configuration and **b** parallel configuration

Table 3 Comparison of experimental and analytical stiffness and Young's modulus of the plymetal

Total stiffness		Young's modulus			
K1 (using E1) (GN/m)	K2 (using E2) (GN/m)	E1		E2	
		Experimental (GPa)	Analytical (GPa)	Experimental (GPa)	Analytical (GPa)
0.335	0.944	3.06	3.41	8.45	9.62

modulus' (E2) because of the presence of localised yielding near voids and pores [38]. The stress-strain curves observed during the uniaxial compression test are presented in Fig. 4. The compression test for all three samples showed two different linear curves before the yielding or non-linear behaviour started. In order to estimate E1 and E2 of the samples, lines were fitting on the segmented data, using the least square method, as shown in Fig. 5. R^2 value is a measure of how close the data are to the fitted line. The curve fitting with the highest R^2 value on the segmented data set points was selected as shown in Table 2. R^2 value is used to find the end point of E1, start of E2 and yield stress of the samples. The values of E1, E2, yield stress and yield strain of the each sample are summarised in Table 2. Young's modulus and the yield strength of the plymetal were found to be more close to the softer 316L stainless steel than harder H13 tool steel.

It should be noted that there is a limited literature available on the compression tests of the solid metal samples made by AM techniques. The parts manufactured by laser deposition may contain many defects such as voids and cracks that are formed during solidification and remelting for depositing the next layer. Thus, their properties are low compared to their wrought counterpart. In addition, if there is any oxidation of metal powder, it will reduce the strength of the alloys [38]. A comparison can be made for the parts manufactured by laser metal deposition and rocks, as both having crystal structures, grain boundaries, voids and discontinuities. A similar behaviour can be observed for the compressive tests of rocks [40]. The initial deflection in the sample during the uniaxial compression is the combination of deformation of the sample, interface with platens and the spherical seat of the machine to stabilise axial loading. In addition, the small defects take the major load during initial sample loading, resulting in highly localised stress levels, in spite of calculated mean stress acting on the whole sample being low [40]. The overall effect resulted in the non-linearity during uniaxial compressive testing before yielding.

Riza et al. [36] have also reported earlier that dual modulus of the elasticity was observed in the region before the yielding during the tensile tests for solid steel samples manufactured by the same DMD machine. In those testing procedures, a low strain rate (0.001/s) was used for both H13 and 316L samples. E1 and E2 values are lower than those reported earlier [36] because totally different operational parameters were used to manufacture those samples. It is a known phenomenon that changing process parameters during DMD has resulted in a different outcome of the material in terms of microstructure, grain size, porosity and hardness [41, 42].

Table 4 Average microhardness value of all samples before and after the compression test

	Before test (HV)	After test (HV)	Difference (%)
316L in plymetal	388	408	+5%
H13 in plymetal	668	725	+8%
316L sample	385	400	+4%
H13 sample	685	722	+5%

3.2 Analytical solution of elastic properties of the plymetal

To calculate the uniaxial Young's modulus of the plymetal analytically, a stiffness method was used. This method is applicable within the elastic domain considering the extension analogous to a spring having stiffness (K), which is given by Eq. 1. In this equation, A is a uniform cross-sectional area, E is

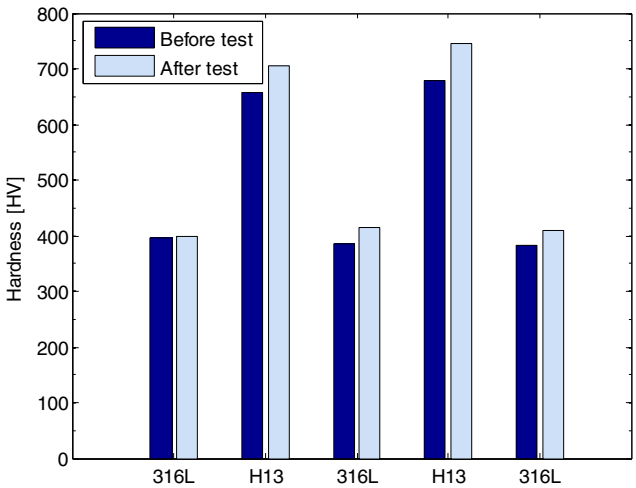

Fig. 8 Vickers microhardness on the plymetal surface, before and after the compression test from centre towards outside in radial direction

Table 5 Comparison of microhardness values with the available literature

	Scan speed (mm/s)	Feed rate (mg/s)	Laser power density (W/mm^2)	Microhardness (HVN)
For 316L stainless steel				
Majumdar et al. [41]	5	203	40	280
Amine et al. [42]	5	200	46	275[a]
316L in plymetal	5.4	125	2800	388[b]
316L sample	4.2	208	610	385[b]
For H13 tool steel				
Telasang et al. [43]	5	199.5	255	660[a]
Choi et al. [37]	10.5–19	83–183	2600–3640	520–580
H13 in plymetal	5.4	135	2800	668[b]
H13 sample	4.2	208	610	685[b]

[a] Maximum value

[b] Before compression test

the Young's modulus of the material, and L is the length perpendicular to the cross-sectional area.

$$K = \frac{AE}{L} \tag{1}$$

The whole structure is first divided in the axial direction and then in the radial direction. In the axial direction, each layer zone having the same cross-sectional areas with the alternating materials is in series configuration as shown in Fig. 6. In the radial direction, each layer zone with different cross-sectional areas with alternating materials is in parallel configuration. Each configuration can be represented analogous to the circuit diagram as shown Fig. 7.

Thus, the stiffness in axial direction (K_{a1}) for the inner most metals (Fig. 7a) is a series sum having stiffness as shown in Eq. 2. In Eq. 2, the number subscripts are referring to material position in the plymetal with the first number subscript showing the axial direction (layer zone) and the second number subscript showing the radial direction. For example, 11 is the first bottom material both in axial and in radial directions. Similarly, 31 means third layer zone but the first central material.

$$\frac{1}{K_{a1}} = \frac{1}{K_{a11}} + \frac{1}{K_{a21}} + \frac{1}{K_{a31}} + \frac{1}{K_{a41}} \tag{2}$$

$$\frac{1}{K_{a1}} = \frac{L_{11}}{A_{11}E_A} + \frac{L_{21}}{A_{21}E_B} + \frac{L_{31}}{A_{31}E_A} + \frac{L_{41}}{A_{41}E_B} \tag{3}$$

$$K_{a1} = \frac{A_1}{2L}\left[\frac{E_A E_B}{E_A + E_B}\right] \tag{4}$$

Since, the plymetal has the same cross-sectional area (A_1) and the length (L) for each alternating materials in the axial direction, thus, Eq. 3 can be reduced to Eq. 4. For each annular structure, only the cross-sectional area will be changed. Thus, stiffness value of each annular structure can be calculated using Eq. 4 with modified cross-sectional area. There are now five stiffness values representing combined materials in an annular arrangement. This is now representing a parallel configuration, and the total stiffness (K) of the plymetal is the

Fig. 9 Optical micrograph of the plymetal surface showing periodic melt pools

simple arithmetic sum. Thus, the total stiffness of the plymetal is given by Eq. 5.

$$K = \frac{1}{2L}\left[\frac{E_A E_B}{E_A + E_B}\right]\left\{\sum\nolimits_{n=1}^{5} A_n\right\} \quad (5)$$

After calculating the total stiffness of the plymetal using Eq. 5, Young's modulus of the plymetal can be calculated using Eq. 1 by considering overall cross-sectional area and total thickness of the sample. The values of the total stiffness of the plymetal calculated using E1 and E2 of the H13 and 316L samples and the corresponding Young's modulus of the plymetal are summarised in Table 3. The analytical values tend to be higher than those found experimentally, as the stiffness method does not cater for the interface effect between the two metals and the possible defects during manufacturing. For the possible applications of the proposed plymetal, analytical calculations should be considered as higher guideline values and conservative approach should be used for considering stiffness of the plymetal.

3.3 Hardness measurements

The Vickers microhardness number (HVN) was conducted on the top surface of the samples with 100-g force using a Buehler microhardness testing machine. The average values of hardness on the top surface of all three samples before and after the uniaxial compression tests are shown in Table 4.

Once the metal goes beyond the yield point in compression test, it gets hardened because of the strain hardening. As the load applied was beyond the yield stress in all three samples, the HVN of the samples was found to have increased by more than 4%. For the plymetal, the hardness values of the two metals in the top surface before and after the compression test are shown in Fig. 8. The maximum strain applied on the plymetal was 0.135 greater than the yield strain that was found to be 0.087. The inner most portions may be subjected to the highest stress due to the smallest cross-sectional area. However, because of the confinement, there was less straining in it, resulting in less hardening compared to the annular structures, which have more liberty to expand radially during the compression test.

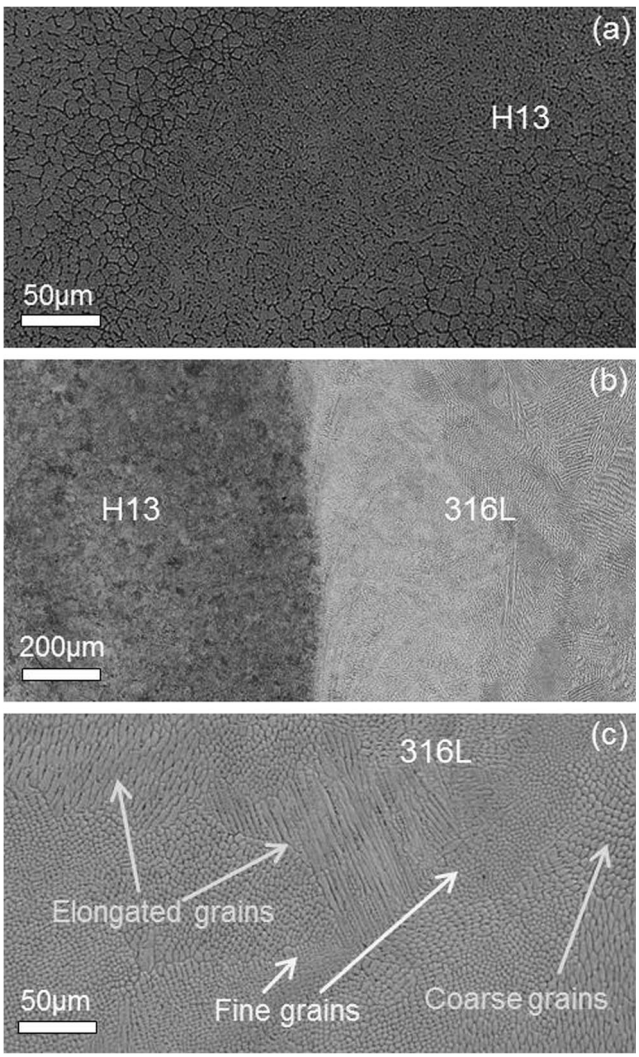

Fig. 10 Optical micrograph of the plymetal surface showing microstructure in **a** H13, **b** interface and **c** 316L regions

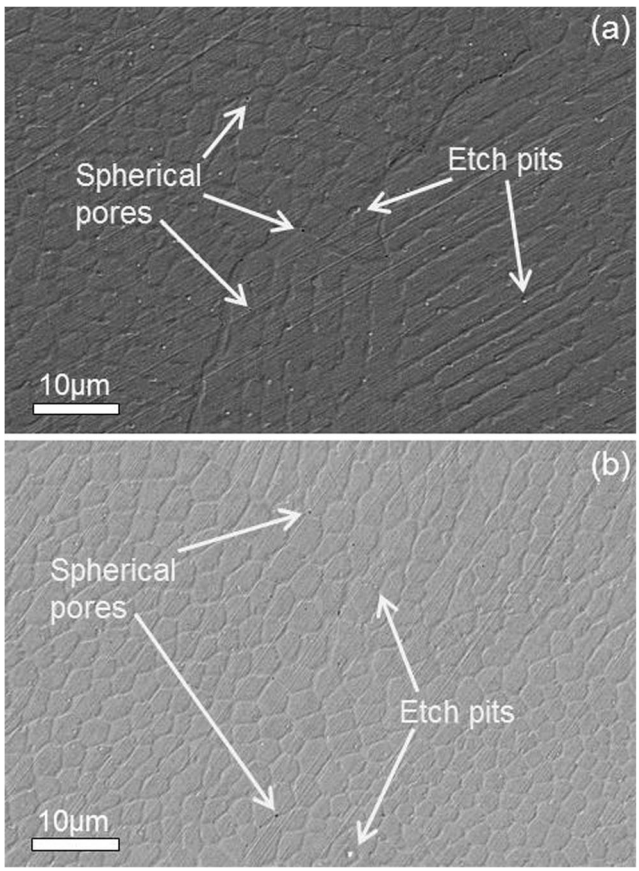

Fig. 11 SEM micrograph of the plymetal in **a** H13 region and **b** 316L region

The HVN values of plymetal materials are also compared with the available hardness values in literature of the same materials processed by laser deposition as summarised in Table 5. The HVN values of both metals in plymetal are found to be higher than the reported values of hardness even for the different laser power densities used. However, it has been reported for H13 that during deposition, fine lath martensite and carbides are formed, which are responsible for increasing hardness in laser deposition compared to bulk H13 tool steel [43].

3.4 Microstructure analysis

In laser deposition of metals, the thermal history experienced during processing is directly related to different microstructures formed and thus to the mechanical properties of the final material. Periodic uniform melt pools along with the overlapping regions were observed in optical microscopy generated by the scanning laser beam during metal powder deposition as shown in Fig. 9. The grain growth was even across the melt pool, mostly due to remelting or formation of heat-effected zones at the boundary of the solidifying melt pool after the laser beam moved forward.

The optical micrographs of the plymetal at higher resolution are shown in Fig. 10 at H13 and 316L deposited regions. After the chemical etching, H13 tool steel grains were dark in colour and 316L stainless steel grains were light in colour. Similar microstructure was also observed in laser deposition of H13 tool steel [43] and 316L stainless steel [44]. Elongated, coarse grains and fine grains were observed during the microstructure analysis because of the high cooling rates and non-equilibrium conditions. High cooling rates are possible during laser AM technologies [23]. As shown in Fig. 10b, at the bond interface between the two metals, the shape and size of grains change with very little dilution resulting in a neat interface, which is a product of reintroduction of heat to the previous layer while depositing the next layer. It is considered as a full remelt on the surface and partial remelt in the sub-surface zone also known as the heat-affected zone. The SEM micrographs at higher resolution for H13 and 316L in plymetal are shown in Fig. 11. The microstructures of the plymetal revealed solid structure with negligible porosity. However, small spherical pores of size less than 1 μm were observed on the surface, which may be due to the oxidation during laser deposition. Additionally, etch pits were also observed due to pitting attack of acid etchant. For each layer in vertical direction, the deposition is made in a circular manner with increments in radial direction. During microstructure analysis, no apparent gaps were observed on the etched surface of the sample. Additionally, at the boundary of the two materials, a perfect bonding was observed mainly because of the half-track overlapping used during the laser deposition.

4 Conclusion

A novel plymetal concept is presented with alternating layers of metals both in the radial and in the axial directions. The plymetal, which consisted of H13 tool steel and 316L low-carbon stainless steel, was manufactured by laser-assisted DMD AM technology. A uniaxial compression test was performed to estimate Young's modulus, yield strength and yield strain of the plymetal. The dual modulus of elasticity in the region before yielding was observed for the plymetal as well as for the samples of H13 tool steel and 316L stainless steel. The dual Young's modulus of the plymetal was found to be as E1 = 3.06 GPa and E2 = 8.45 GPa. The yield strength and yield strain of the plymetal were found to be 600 MPa and 0.087, respectively. An analytical equation to calculate Young's modulus of the plymetal based on the stiffness method was also derived. The analytical Young's modulus value for the plymetal was found to be marginally higher than the experimental values. Vickers microhardness of the individual metal in the plymetal was also observed before and after the compression test. The microstructure of the plymetal was observed through optical and scanning electron microscopy, which revealed perfect bonding between the two metals. The size of the pores in the plymetal was found to be less than 1 μm. More specialised plymetals can be designed and manufactured using AM by changing the dimensions, the number of materials and in the fashion that they can be altered to give better tuneable control on the mechanical properties in such composite structures for numerous applications.

Acknowledgements Sohaib Z Khan is thankful for Endeavour Fellowship, Government of Australia, for the support and completion of this work. The authors would like to thank Mr. Girish Thipperudruppa for his support in DMD and Dr. M Awais Javed for his support in microscopic analysis.

References

1. Gibson LJ, Ashby MF (1997) Cellular solids: structure and properties, 2 edn. Cambridge University Press, UK
2. Ryan G, Pandit A, Apatsidis DP (2006) Fabrication methods of porous metals for use in orthopaedic applications. Biomaterials 27(13):2651–2670. doi:10.1016/j.biomaterials.2005.12.002
3. Nakajima H (2007) Fabrication, properties and application of porous metals with directional pores. Prog Mater Sci 52(7):1091–1173. doi:10.1016/j.pmatsci.2006.09.001
4. Kaczmar JW, Pietrzak K, Włosiński W (2000) The production and application of metal matrix composite materials. J Mater Process Technol 106(1–3):58–67. doi:10.1016/S0924-0136(00)00639-7
5. Hall IW, Tasdemirci A, Derrick J (2009) Quasi-static and high strain rate properties of a cross-ply metal matrix composite. Mater Sci Eng A 507(1–2):93–101. doi:10.1016/j.msea.2008.12.021
6. Wang J, Li L, Tao W (2016) Crack initiation and propagation behavior of WC particles reinforced Fe-based metal matrix composite produced by laser melting deposition. Optics Laser Technol 82:170–182. doi:10.1016/j.optlastec.2016.03.008

7. Zhang X, Zhang Q, Hu H (2014) Tensile behaviour and microstructure of magnesium AM60-based hybrid composite containing Al2O3 fibres and particles. Mater Sci Eng A 607:269–276. doi:10.1016/j.msea.2014.03.069
8. Güden M, Akil O, Tasdemirci A, Çiftçioglu M, Hall IW (2006) Effect of strain rate on the compressive mechanical behavior of a continuous alumina fiber reinforced ZE41A magnesium alloy based composite. Mater Sci Eng A 425(1–2):145–155. doi:10.1016/j.msea.2006.03.028
9. Kee Paik J, Thayamballi AK, Sung Kim G (1999) The strength characteristics of aluminum honeycomb sandwich panels. Thin-Walled Struct 35(3):205–231. doi:10.1016/S0263-8231(99)00026-9
10. Ferreira ADBL, Nóvoa PRO, Marques AT (2016) Multifunctional material systems: a state-of-the-art review. Compos Struct. doi:10.1016/j.compstruct.2016.01.028
11. Kieback B, Neubrand A, Riedel H (2003) Processing techniques for functionally graded materials. Mater Sci Eng A 362:81–105
12. Shaw MC, Marshall DB, Dadkhah MS, Evans AG (1993) Cracking and damage mechanisms in ceramic/metal multilayers. Acta Metall Mater 41(11):3311–3322. doi:10.1016/0956-7151(93)90060-6
13. Hashim J, Looney L, Hashmi MSJ (1999) Metal matrix composites: production by the stir casting method. J Mater Process Technol 92–93:1–7. doi:10.1016/S0924-0136(99)00118-1
14. Tsuji N, Saito Y, Lee SH, Minamino Y (2003) ARB (accumulative roll-bonding) and other new techniques to produce bulk ultrafine grained materials. Adv Eng Mater 5(5):338–344
15. Mozaffari A, Manesh HD, Janghorban K (2010) Evaluation of mechanical properties and structure of multilayered Al/Ni composites produced by accumulative roll bonding (ARB) process. J Alloys Compd 489(1):103–109
16. Balasubramanian M (2015) Development of processing windows for diffusion bonding of Ti–6Al–4 V titanium alloy and 304 stainless steel with silver as intermediate layer. Trans Nonferrous Metals Soc China 25(9):2932–2938. doi:10.1016/S1003-6326(15)63919-X
17. Yongqiang D, Guangmin S, Lijing Y (2015) Impulse pressuring diffusion bonding of titanium to stainless steel using a copper interlayer. Rare Metal Mater Eng 44(5):1041–1045. doi:10.1016/S1875-5372(15)30063-1
18. Masood SH (2014) Introduction to advances in additive manufacturing and tooling. Compr Mater Proc:1–2. doi:10.1016/b978-0-08-096532-1.01016-5
19. Pinkerton AJ (2016) [INVITED] Lasers in additive manufacturing. Optics Laser Technol 78, Part A:25–32. doi:10.1016/j.optlastec.2015.09.025
20. Frazier WE (2014) Metal additive manufacturing: a review. J Mater Eng Perform 23(6):1917–1928. doi:10.1007/s11665-014-0958-z
21. Soodi M, Masood SH, Brandt M (2013) Thermal expansion of functionally graded and wafer-layered structures produced by laser direct metal deposition. Int J Adv Manuf Technol 69(9):2011–2018. doi:10.1007/s00170-013-5157-9
22. Syed WUH, Pinkerton AJ, Liu Z, Li L (2007) Coincident wire and powder deposition by laser to form compositionally graded material. Surf Coat Technol 201(16–17):7083–7091. doi:10.1016/j.surfcoat.2007.01.020
23. Verhaeghe F, Craeghs T, Heulens J, Pandelaers L (2009) A pragmatic model for selective laser melting with evaporation. Acta Mater 57(20):6006–6012. doi:10.1016/j.actamat.2009.08.027
24. Soodi M, Masood SH, Brandt M (2014) Tensile strength of functionally graded and wafer layered structures produced by direct metal deposition. Rapid Prototyp J 20(5):360–368. doi:10.1108/RPJ-02-2013-0014
25. Imran MK, Masood SH, Brandt M, Bhattacharya S, Mazumder J (2011) Direct metal deposition (DMD) of H13 tool steel on copper alloy substrate: evaluation of mechanical properties. Mater Sci Eng A 528(9):3342–3349. doi:10.1016/j.msea.2010.12.099
26. Erinosho MF, Akinlabi ET, Pityana S (2015) Influence of processing parameters on laser metal deposited copper and titanium alloy composites. Trans Nonferrous Metals Soc China 25(8):2608–2616. doi:10.1016/S1003-6326(15)63882-1
27. Pulugurtha SR (2014) Functionally graded Ti6Al4V and Inconel 625 by laser metal deposition. PhD thesis. Missouri University of Science and Technology, USA
28. Shah K, Haq I, Khan A, Shah SA, Khan M, Pinkerton AJ (2014) Parametric study of development of Inconel-steel functionally graded materials by laser direct metal deposition. Mater Des 54(0):531–538. doi:10.1016/j.matdes.2013.08.079
29. Balla VK, DeVasConCellos PD, Xue W, Bose S, Bandyopadhyay A (2009) Fabrication of compositionally and structurally graded Ti-TiO_2 structures using laser engineered net shaping (LENS). Acta Biomater 5:1831–1837
30. Liu W, DuPont IN (2003) Fabrication of functionally graded TiC/Ti composites by laser engineered net shaping. Scr Mater 48:1337–1342
31. Articek U, Milfelner M, Anzel I (2013) Synthesis of functionally graded material H13/Cu by LENS technology. Adv Prod Eng Manag 8(3):169–176
32. Wang F, Mei J, Wu X (2007) Compositionally graded Ti6Al4V + TiC made by direct laser fabrication using powder and wire. Mater Des 28:2040–2046
33. Hofmann DC, Roberts S, Otis R, Kolodziejska J, Dillon RP, J-o S, Shapiro AA, Liu Z-K, Borgonia J-P (2014) Developing gradient metal alloys through radial deposition additive manufacturing. Scientific reports 4. doi:10.1038/srep05357
34. Chiu WK, Yu KM (2008) Multi-criteria decision-making determination of material gradient for functionally graded material objects fabrication. Proc. IMechE Part B: Eng Manuf 222:293–307. doi:10.1243/09544054JEM831
35. Hofmann DC, Kolodziejska J, Roberts S, Otis R, Dillon RP, Suh J-O, Liu Z-K, Borgonia J-P (2014) Compositionally graded metals: a new frontier of additive manufacturing. J Mater Res 29(17):1899–1910. doi:10.1557/jmr.2014.208
36. Riza SH, Masood SH, Wen C, Ruan D, Xu S (2014) Dynamic behaviour of high strength steel parts developed through laser assisted direct metal deposition. Mater Des 64(0):650–659. doi:10.1016/j.matdes.2014.08.026
37. Choi J, Chang Y (2005) Characteristics of laser aided direct metal/material deposition process for tool steel. Int J Mach Tools Manuf 45(4–5):597–607. doi:10.1016/j.ijmachtools.2004.08.014
38. Straffelini G, Fontanari V, Molinari A (1999) True and apparent Young's modulus in ferrous porous alloys. Mater Sci Eng A 260(1–2):197–202. doi:10.1016/S0921-5093(98)00960-5
39. Moon JR (1989) Elastic moduli of powder metallurgy steels. Powder Metall 32(2):132–139
40. Korinets A, Alehossein H (2002) Technical note on the initial non-linearity of compressive stress-strain curves for intact rock. Rock Mech Rock Engng 35(4):319–328. doi:10.1007/s00603-002-0030-4
41. Majumdar JD, Pinkerton A, Liu Z, Manna I, Li L (2005) Microstructure characterisation and process optimization of laser assisted rapid fabrication of 316L stainless steel. Appl Surf Sci 247(1–4):320–327. doi:10.1016/j.apsusc.2005.01.039
42. Amine T, Newkirk JW, Liou F (2014) Investigation of effect of process parameters on multilayer builds by direct metal deposition. Appl Therm Eng 73(1):500–511. doi:10.1016/j.applthermaleng.2014.08.005
43. Telasang G, Dutta Majumdar J, Padmanabham G, Tak M, Manna I (2014) Effect of laser parameters on microstructure and hardness of laser clad and tempered AISI H13 tool steel. Surf Coat Technol 258(0):1108–1118. doi:10.1016/j.surfcoat.2014.07.023
44. Casati R, Lemke J, Vedani M Microstructure and fracture behavior of 316L austenitic stainless steel produced by selective laser melting. J Mater Sci Technol. doi:10.1016/j.jmst.2016.06.016